Catalysis Science & Technology

CO_2 capture in the presence of O_2 and selective hydrogenation to CO over Ag-K dual functional material (DFM): Comparative investigation with Cu-based DFM

Journal:	*Catalysis Science & Technology*
Manuscript ID	CY-ART-12-2024-001497.R1
Article Type:	Paper
Date Submitted by the Author:	18-Feb-2025
Complete List of Authors:	Shukuya, Soma; Kogakuin University - Hachioji Campus Hashimoto, Hideki; Kogakuin University, Department of Applied Chemictry Namiki, Norikazu; Kogakuin University - Hachioji Campus Maeno, Zen; Kogakuin University, School of Advanced Engineering

CO_2 capture in the presence of O_2 and selective hydrogenation to CO over Ag-K dual functional material (DFM): Comparative investigation with Cu-based DFM

Soma Shukuya[a], Hideki Hashimoto[a,b,c], Norikazu Namiki[a], Zen Maeno*[a,c]

[a]School of Advanced Engineering, Kogakuin University, 2665-1, Nakano-machi, Hachioji, Tokyo, 192-0015, Japan

[b]Center for Basic Research on Materials, National Institute for Materials, Science, 1-2-1, Sengen, Tsukuba, Ibaraki 305-0047, Japan

[c]PRESTO, Japan Science and Technology Agency (JST), Kawaguchi, Saitama, 332-0012, Japan

*Corresponding author

Zen Maeno, E-mail: zmaeno@cc.kogakuin.ac.jp

Abstract

The CO_2 capture and reduction (CCR) over dual-functional materials (DFMs) is promising as an alternative utilization strategy of low-concentration CO_2 in exhaust gases and/or air. Despite much effort toward the development of DFMs for CH_4 formation through CCR, the study of DFMs for CO formation has been less reported. Especially, the DFMs workable under milder reaction temperature and O_2 co-existed conditions has been rarely developed. In this work, Ag-based DFMs were investigated for CO_2 capture in the presence of O_2 and selective hydrogenation to CO. Ag and K co-loaded Al_2O_3 exhibited the best CO formation performance among different alkaline (earth) metal co-loaded materials. The O_2 compatibility of Ag-K/Al_2O_3 was also studied by comparing with Cu-K/Al_2O_3. The reduced Cu species were oxidized by O_2 into Cu oxides, and thus the reduction of Cu species after gas switching to H_2 occurred. In contrast, the reduced Ag state was maintained even after CO_2 capture in the presence of O_2 over Ag-K/Al_2O_3, which results in the suppression of water formation after gas switching to H_2 and consecutive desorption of captured CO_2. The distinct O_2 compatibility is ascribed to the different redox properties between Cu-K/Al_2O_3 and Ag-K/Al_2O_3.

Introduction

To achieve a carbon-neutral society by 2050, technologies must be developed for the reduction of CO_2 emissions. The treatment of exhaust gases from thermal power and chemical plants via CO_2 capture and storage (CCS) has garnered significant attention.[1–3] However, the CO_2 stored using this method is potentially released into the atmosphere. CO_2 capture and utilization (CCU) is an alternative strategy to CCS, and various CO_2 conversion technologies have also been studied. In general, an additional reactor is required to separate and purify CO_2 from a gas mixture containing other components, such as O_2.[4–9] CO_2 capture and reduction (CCR) using H_2 over dual-functional materials (DFMs) has recently attracted attention as an alternative approach for CO_2 utilization. The CCR process is an unsteady operation in which gases containing low concentrations of CO_2 and hydrogen are fed alternately over DFMs with CO_2 absorption and hydrogenation capabilities. In theory, CO_2 absorption is not inhibited by O_2; additionally, the absorbed CO_2 can be directly converted into methane and/or CO. Therefore, CCR is a promising method that can address the challenges of conventional CCU. [10–14]

Since the study of Farrauto et al., numerous studies on CH_4 synthesis using DFMs have been reported.[15–17] Although CO is more useful than CH_4 in chemical synthesis, there are few reports on the selective formation of CO via CCR.[18–25] Methanation is thermodynamically favorable at low temperatures; however, the conversion of CO_2 to CO is endothermic. The development of DFMs for the formation of CO via CCR, particularly under mild reaction conditions, is challenging. The first study of CO synthesis via CCR was achieved by Urakawa et al using an FeCrCu-K-based DFM at 450–550 °C.[18] Ni-based catalysts and Fe5Co5Mg10CaO have been shown to be effective for CO production. However, these catalysts require temperatures above 600 °C. Although Ni-Rb/Al_2O_3[21] and Na/Al_2O_3[22] have been reported as bifunctional catalysts that operate at temperatures of approximately 400 °C, there are few examples of catalysts that function at approximately 300 °C. The activity of Cu-K/Al_2O_3 DFMs has been demonstrated in the selective synthesis of CO via CCR under O_2-free conditions[23]. However, the presence of O_2 in a simulated low-concentration CO_2 gas causes the production of H_2O via the H_2 reduction of CuO. This results in the desorption of the carbonate on the surface of the catalyst, leading to deactivation.[24] Pt–Na-based bifunctional catalysts are examples of operational DFMs in the presence of O_2.[25] Pt-Na-based bifunctional catalysts are durable for long periods; however, concerns remain regarding the use of expensive platinum group metal (PGM) elements. Unfortunately, PGM-free catalysts that are effective for CO production via CCR in the presence of O_2 at temperatures of approximately 300 °C are not yet developed.

CO and/or formic acid are intermediates for the synthesis of CH_3OH via CO_2 hydrogenation using Ag- and Cu-based catalysts.[26] The standard electrode potential of Ag ($E°$ = 0.799 V) is higher than that of Cu ($E°$ = 0.337 V), and Ag_2O is unstable under heating conditions; therefore, the ease of oxidation of Ag is theoretically lower than that of Cu. Ag-based DFMs would facilitate CO production via CCR even in the presence of O_2, overcoming practical problems of the reported DFMs for CO production under mild conditions such as the deactivation by O_2 and the use of expensive raw materials. In this study, the CCR capabilities of Ag-K/Al_2O_3 and Cu-K/Al_2O_3 in the absence or presence of O_2 at 350 °C were assessed. Ag-K/Al_2O_3 produced a higher quantity of CO in the presence of O_2 than that of Cu-K/Al_2O_3. The factors influencing the improved performance of the Ag-based DFM were assessed through characterization using X-ray diffraction (XRD) and temperature-programmed reduction (H_2-TPR). The CCR capacity of a combined Ag- and Cu-K/Al_2O_3 system was also examined to discuss the origin of O_2 compatibility of Ag-K/Al_2O_3.

Experimental

Catalyst preparation and characterization

All DFMs were synthesized using the sequential impregnation method. 1 g of Al_2O_3 (PURALOX SBa 200; SASOL Ltd.) was added to an aqueous solution containing 0.207 g of KNO_3 (FUJIFILM Wako). Subsequently, the suspension was heated to evaporation at 50 °C in a vacuum pump and then dried overnight at 100 °C. The resulting solid was calcined at 500 °C for 2 h in air to produce K-loaded Al_2O_3 (K/Al_2O_3, K: 8 wt.%). 0.157 g of $AgNO_3$ (FUJIFILM Wako) was then impregnated into K/Al_2O_3 (Ag: 10 wt.%) to obtain Ag-K/Al_2O_3. Ag-K/Al_2O_3 was further treated under 20 % H_2/N_2 flow at 350 °C for the CCR reaction and characterization. Other Al_2O_3-supported Ag-based DFMs and Cu-K/Al_2O_3 (Cu: 10wt%) were prepared in a similar manner.

XRD measurement was performed using Cu-Kα radiation on a Rigaku MiniFlex600. Transmission electron microscopy (TEM) images were obtained using a JEOL JEM-2100 microscope with energy dispersive X-ray spectroscopy (EDS, JEOL JED-2300T). X-ray photoelectron spectroscopy (XPS) measurement was conducted using JEOL JPS-9030 employing Mg Kα radiation. Charge correction was referenced using the O 1s peak at 532.0 eV. H_2-TPR experiments were carried out using MicrotracBEL BELCAT II. The water formation via redox reaction of metal species was monitored by a quadrupole mass spectrometry, Ulvac BGM2-102.

CCR operation

Figure S1 shows the equipment for the CCR. A DFM (100 mg) was heated in a quartz

reactor to 350 °C using an electric furnace in the presence of a mixed gas that contained a low concentration of CO_2 (100 mL/min of 1 % CO_2+20 % O_2/N_2). Subsequently, the DFMs was pretreated for 30 min using H_2 gas (100 mL/min of 20 % H_2/N_2). The CCR operation was then conducted by alternating the gas flow between 1 % CO_2 + 20 % O_2/N_2 and 20 % H_2/N_2 every 5 min using a timer-controlled four-way valve under isothermal conditions (350 °C). The generated CO, CH_4 and unadsorbed CO_2 in the outlet gas were quantitatively analyzed using Fourier transform infrared (FTIR) spectroscopy. The unadsorbed CO_2, and generated CO and CH_4 were quantitatively analyzed at peak areas of 2395–2235, 2250–2001, and 3031–2994 cm^{-1}, respectively. The amounts of adsorbed CO_2 (Ad_{CO2}), generated CO/CH_4 (Q_{CO}), and CO selectivity (S_{CO}) were quantified using the following equations. The conversion value of absorbed CO_2 ($Conv_{absCO2}$) was determined based on the amount of generated CO/CH_4 and adsorbed CO_2.

$$Ad_{CO2}[mmol/g] = \frac{1}{W}\int_{t_{CO_2,\,start}}^{t_{CO_2,\,end}} (F_{CO2,in}(t) - F_{CO2,out}(t))dt \quad \cdots (1)$$

$$Q_{CO}[\mathrm{mmol/g}] = \frac{1}{W}\int_{t_{H_2,\,start}}^{t_{H_2,\,end}} F_{CO}(t)dt \quad \cdots (2)$$

$$S_{CO} = \frac{Q_{CO}}{Q_{CH4} + Q_{CO}} \quad \cdots (3)$$

$$Conv_{adsCO2} = \frac{Q_{CH4} + Q_{CO}}{Ad_{CO2}} \quad \cdots (4)$$

Results and Discussion

The several previous studies on DFMs for CCR, co-loaded alkaline (earth) metal species significantly affect the CCR performance.[21,25] In this study, a series of Ag-based DFMs with different alkaline (earth) metal salts [Na, Mg, K, and Ca (the loading amount: approximately 2 mmol/g)] were prepared, and their CCR performance was investigated under the condition in the presence of O_2 during CO_2 capture step. The Ag-K co-loaded DFM, Ag-K/Al_2O_3, showed the best CCR performance and CO selectivity (Figure 1). The formation amount and selectivity of CO were 0.121 mmol/g and 93 %, respectively. The CCR performance decreased in the following order: Ag-K > Ag-Na > Ag-Ca > Ag-Mg/Al_2O_3. Ag-K/Al_2O_3 maintained its good CCR performance for several cycles (Figure S2).

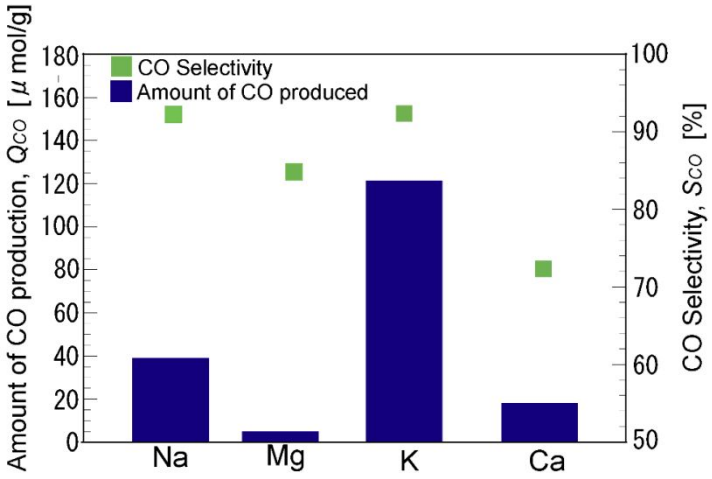

Figure 1 Effect of various alkali metals or alkali earth metals on amount of CO production and CO selectivity in CCR using Ag/Al_2O_3-based dual function catalysts.

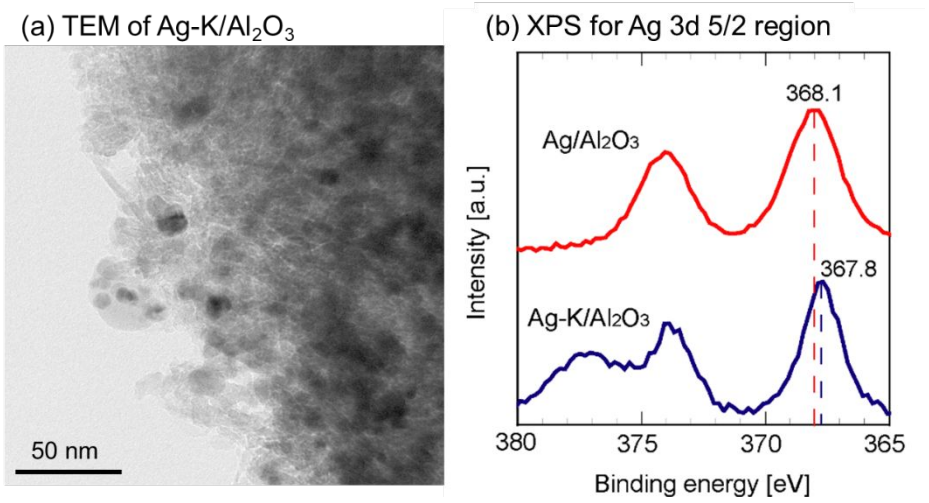

Figure 2. (a) TEM image of $Ag\text{-}K/Al_2O_3$ and (b) XPS spectra for Ag 3d 5/2 region of Ag/Al_2O_3 and $Ag\text{-}K/Al_2O_3$.

The XRD measurement of $Ag\text{-}K/Al_2O_3$ revealed the clear diffraction pattern of metallic Ag whereas no diffraction peak assignable to K compounds was observed, indicating the highly dispersion of K species (vide infra). The TEM observation of $Ag\text{-}K/Al_2O_3$ showed the formation of Ag nanoparticles with average diameter of approximately 17 nm (Figure 2a (Different TEM images of $Ag\text{-}K/Al_2O_3$ are shown in Figure S3)). The EDS analysis of $Ag\text{-}K/Al_2O_3$ was not suitable to analysis of dispersion of K species due to overlap of Ag-L and K-K signals (Figure S4). However, the EDS analysis of K/Al_2O_3 showed the atomically dispersion of K species (Figure S5). In X-ray photoelectron spectroscopy (XPS) measurement, the spectra of Ag 3d 5/2 region for $Ag\text{-}K/Al_2O_3$ exhibited the peak at 367.8 eV,

which was slightly lower than that for Ag/Al_2O_3 (368.1 eV) assignable to metallic Ag species (Figure 2b) [27]. This difference was interpreted as the oxidation of Ag particle surface by interaction with dispersed alkaline metal oxides[28]. The XPS spectra for K 2p 3/2 region for $Ag\text{-}K/Al_2O_3$ indicated the presence of monovalent K species rather than metallic K (Figure S6). The surface composition ratio of Ag for $Ag\text{-}K/Al_2O_3$ was much lower than that for Ag/Al_2O_3 (Table S1) while the surface composition ratio of K for $Ag\text{-}K/Al_2O_3$ and K/Al_2O_3 were similar, supporting the interaction of Ag nanoparticles and dispersed K oxide species.

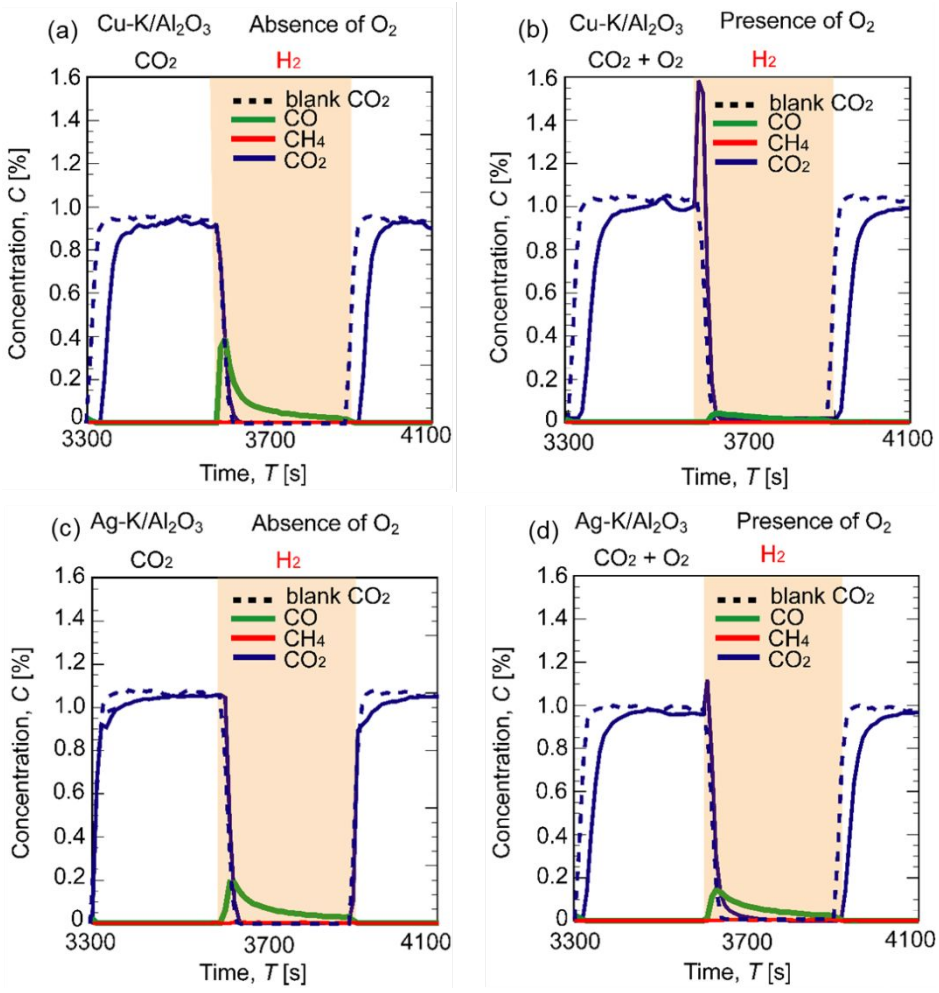

Figure 3. Concentration profile of CO_2, CH_4, and CO during CCR using (a, b) Cu- or (c ,d) $Ag\text{-}K/Al_2O_3$ in (a, c) absence or (b, d) presence of O_2.

To investigate the O_2 compatibility of $Ag\text{-}K/Al_2O_3$, the CCR performance of $Ag\text{-}K/Al_2O_3$ and $Cu\text{-}K/Al_2O_3$ were compared in the presence or absence of O_2. The concentration profiles of the effluent gas from the CCR process under different conditions are shown in Figure 3. In CCR using $Cu\text{-}K/Al_2O_3$ in the absence of O_2, the duration of CO_2 adsorption and considerable

CO formation were observed under CO_2/N_2 and H_2/N_2 flows, respectively (Figure 3a). However, the formation of CO significantly decreased in the presence of O_2 (Figure 3b). In addition, a CO_2 desorption peak was observed after the gas flow was switched from CO_2+O_2/N_2 to H_2/N_2. The deactivation of Cu-K/Al_2O_3 in the presence of O_2 was similar to the results of a previous study[24]. In contrast, the Ag-K/Al_2O_3 catalyst exhibited a favorable CO formation performance even in the presence of O_2 although its performance slightly decreased in the presence of O_2 (Figure 3c and d).

Table 1 CCR performance of Ag- and Cu-K/Al_2O_3 in the presence and absence of O_2.

DFM	O_2	Ad_{CO2} [a] [mmol/g]	Q_{CO} [a] [mmol/g]	C_{CO_Max} [a] [ppm]	S_{CO} [b] [%]	$Conv_{adCO2}$ [b] [%]
Cu-K/Al_2O_3	presence	0.106	0.053	507	99	51
	absence	0.176	0.171	3824	99	98
Ag-K/Al_2O_3	presence	0.141	0.121	1446	93	92
	absence	0.173	0.166	1753	96	99

Reaction conditions: 0.1 g of DFM, 350 °C, 100 mL/min of 1 % CO_2 + 20 % O_2/N_2 for 5 min, followed by 100 mL/min of 20 % H_2 /N_2 for 5 min. [a] Composition of the effluent gas at the outlet was quantitatively analysed using FTIR spectroscopy combined with a gas cell. See the Experimental section. [b] Based on the amount of CO and CH_4 generated during the reduction period.

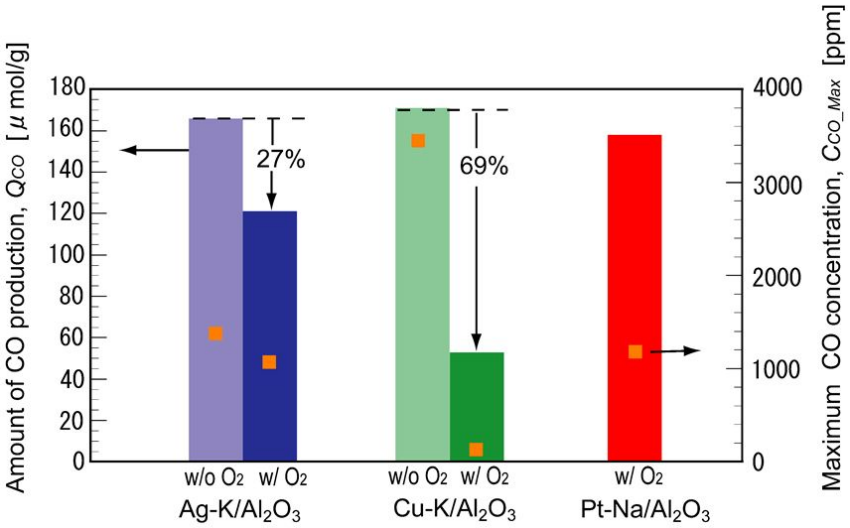

Figure 4. Quantity of CO produced during CCR in the absence or presence of O_2 followed by hydrogenation using Ag-K/Al_2O_3 , Cu-K/Al_2O_3 , and Pt-Na/Al_2O_3. The CO formation performance of Pt-Na/Al_2O_3 was obtained from the previous paper[25].

The detailed CCR performances of Ag- and Cu-K/Al_2O_3 in the absence and presence of O_2 are summarized in Table 1. The quantities and maximum concentrations of CO under different conditions are shown in Figure 4. The quantity of CO (166 μmol/g) formed using the Ag-K/Al_2O_3 catalyst under O_2 free conditions was marginally lower than that of Cu-K/Al_2O_3 (177 μmol/g). In contrast, the performance of Ag-K/Al_2O_3 (121 μmol/g) was superior to that of Cu-K/Al_2O_3 (53 μmol/g) in the presence of O_2. The maximum CO concentration of Cu-K/Al_2O_3 decreased from 3824 to 507 ppm in the presence of O_2. Although the maximum CO concentration of Ag-K/Al_2O_3 under O_2 free conditions was lower than that of Cu-K/Al_2O_3, a higher maximum CO concentration was obtained in the presence of O_2 (1446 ppm). The CO formation amount and maximum concentration for Ag-K/Al_2O_3 decreased by 27 % and 18 %, respectively. In contrast, the formation amount and maximum concentration of CO decreased by 69 and 87 %, respectively, when using the Cu-K/Al_2O_3 catalyst. This showed that O_2 deactivation was suppressed at the Ag-K/Al_2O_3 catalyst, but not at Cu-K/Al_2O_3. Under all conditions, CO selectivity was excellent over 90 %. Although the formation amount and maximum concentration of CO produced using Ag-K/Al_2O_3 (121 μmol/g and 1446 ppm, respectively) were marginally lower than those produced using Pt-Na/Al_2O_3 (163 μmol/g and 1554 ppm, respectively),[25] Ag-K/Al_2O_3 performs as a O_2-compatible DFM for CCR to synthesize CO under mild conditions. Regarding the stoichiometry of the amount of CO_2 adsorbed to K loading amount, approximately 10% of loaded K serve as CO_2 capture sites. To evaluate the sustainability of Ag-K/Al_2O_3, the long-term CCR operation was carried out for 20 h (corresponding to 120 cycles) under similar conditions. The effluent gas concentration profiles at 1, 5, 10, 15 and 20 h are shown in Figure S7. The CO formation amount (175-190 mmol/g) and maximum concentration (approximately 2500-2800 ppm) were maintained (Figure S8), confirming the durability of Ag-K/Al_2O_3. To investigate whether the O_2 was mixed with the generated CO or not, the effluent gas of CCR using Ag-K/Al_2O_3 was monitored by FTIR and mass spectrometry. Note that Ar was used as a balance gas for this experiment because mass numbers of N_2 and CO were same. The effluent gas in the initial stage of CO formation contains O_2 (Figure S9). For utilization of the generated CO, the purge step is necessary to separate O_2 and CO.

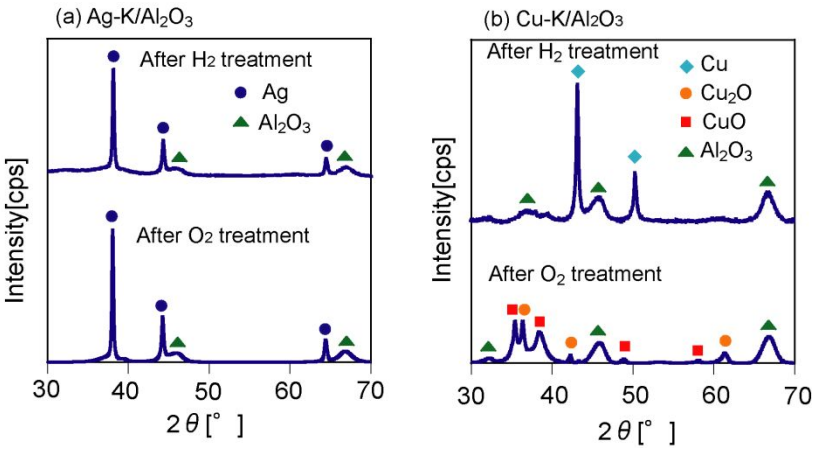

Figure 5. XRD of (a) Ag-K/Al_2O_3 and (b) Cu-K/Al_2O_3 after reduction and after oxidation at 350 °C

Figure 5 shows the XRD analysis of the Ag-K/Al_2O_3 and Cu-K/Al_2O_3 treated under H_2/N_2 flow, followed by O_2/N_2 flow at 350 °C. The diffraction peaks of γ-Al_2O_3 were observed at 2θ values of approximately 37°, 43°, and 67° under all conditions. Using Ag-K/Al_2O_3, diffraction peaks of metallic Ag were observed at 2θ values of approximately 38°, 44°, and 64° after H_2 treatment (Figure 5a). The XRD pattern was maintained after O_2 treatment, indicating that most of the Ag was present in the metallic state, even after the CO_2 adsorption step in the presence of O_2. No diffraction peaks were detected for the K species, suggesting that the K species was dispersed. The XRD measurement of the Ag-K/Al_2O_3 before H_2 treatment was carried out. The diffraction peaks derived from KNO_3 were observed (Figure S10). The H_2 treatment induced the dispersion of K species. Regarding Cu-K/Al_2O_3, diffraction peaks of metallic Cu were observed at 2θ values of approximately 43° and 50° after H_2 treatment (Figure 5b); however, peaks attributed to the oxidized Cu species, such as Cu_2O and CuO, were observed after O_2 treatment. These results showed that the Cu species was oxidized under O_2 flow, whereas most of the Ag species remained in the metallic state under the same conditions.

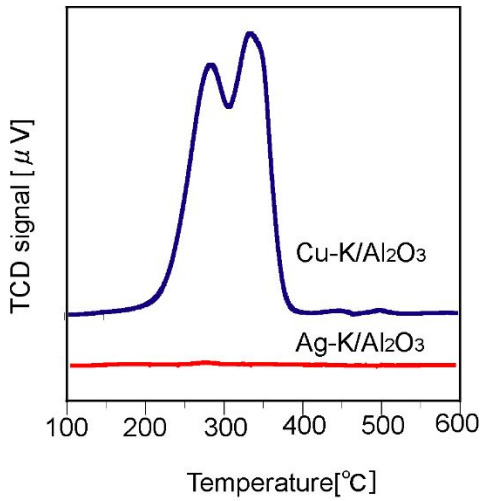

Figure 6. H_2-TPR profiles of Cu(10)K(8)/Al_2O_3 and Ag-K/Al_2O_3

The H_2 TPR profiles of the O_2-treated Ag-K/Al_2O_3 and Cu-K/Al_2O_3 catalysts are shown in Figure 6. Regarding Cu-K/Al_2O_3, two H_2 consumption peaks ascribed to the reduction of CuO and Cu_2O were observed at approximately 270 °C and 340 °C, respectively. The quantity of consumed H_2 was 1.10 mol/g, which was similar to the theoretical value for reducing 10 wt.% of CuO in Cu-K/Al_2O_3 (1.26 mol), indicating that most of the Cu species were oxidized. In contrast, a low quantity of H_2 consumption (0.03 mol/g) was observed at approximately 290 °C using Ag-K/Al_2O_3. Therefore, the Ag species in Ag-K/Al_2O_3 largely remained in its metallic state even after O_2 exposure at 350 °C. The H_2-TPR measurements using Cu and Ag catalysts with varying Cu/Ag loadings of 1 wt%, 5 wt%, and 10 wt%, were additionally carried out (Table S2). In the case of Cu catalyst, when the Cu loading was varied from 1, 5, to 10 wt%, the H_2 consumption amount proportionally increased from 0.20, 0.98 to 1.9 mmol/g, suggesting that almost Cu species were oxidized. On the other hand, in the case of the Ag catalyst, the H_2 consumption amount was 0.019, 0.049, and 0.039 mmol/g for 1, 5, and 10 wt% of Ag loading amount, respectively. The H_2 consumption amount and its trend are quite different from those for Cu-K/Al_2O_3, implying that the surface of Ag species was oxidized and the inside of Ag species was likely to be inert. The slight decrease of CO formation performance in the presence of O_2 might be due to the oxidation of surface of Ag species.

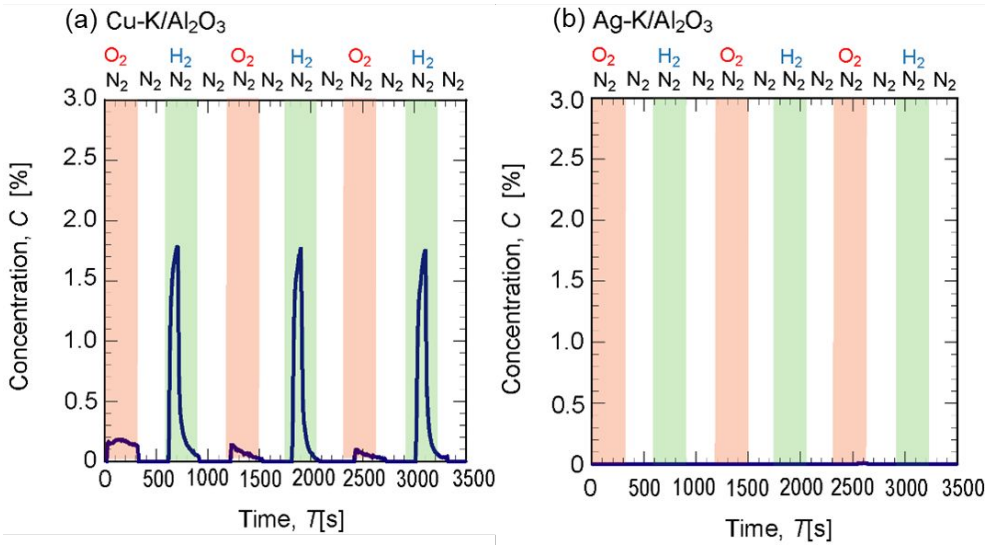

Figure 7. Concentration profiles of water produced in O_2 and H_2 gas switching for (a) Cu-K/Al_2O_3 or (b) Ag-K/Al_2O_3.

In previous studies on the CCR process using Cu-K/Al_2O_3 in the presence of O_2, the H_2O generated through the H_2 reduction of Cu oxides resulted in a loss of CCR performance[23]. To compare H_2O formation between Ag- and Cu-K/Al_2O_3, O_2/N_2 and H_2/N_2 gases were flowed alternately into a reaction tube filled with Cu-K/Al_2O_3 or Ag-K/Al_2O_3 every 5 min. The generated H_2O was monitored using mass spectrometry (m/z = 18) (Figure 7). N_2 was purged before gas switching to prevent the reaction of H_2 with O_2. A peak was observed by switching O_2 to H_2, confirming the formation of H_2O through H_2 reduction of the Cu oxides. A relatively low quantity of H_2O was also detected when the H_2 gas was switched to O_2, which could be ascribed to the reaction of O_2 with the adsorbed H species. In contrast, the peak derived from H_2O was rarely observed for Ag-K/Al_2O_3 when alternatively switching the gas between O_2 and H_2. This contrasting result is consistent with observations from the XRD and H_2-TPR experiments.

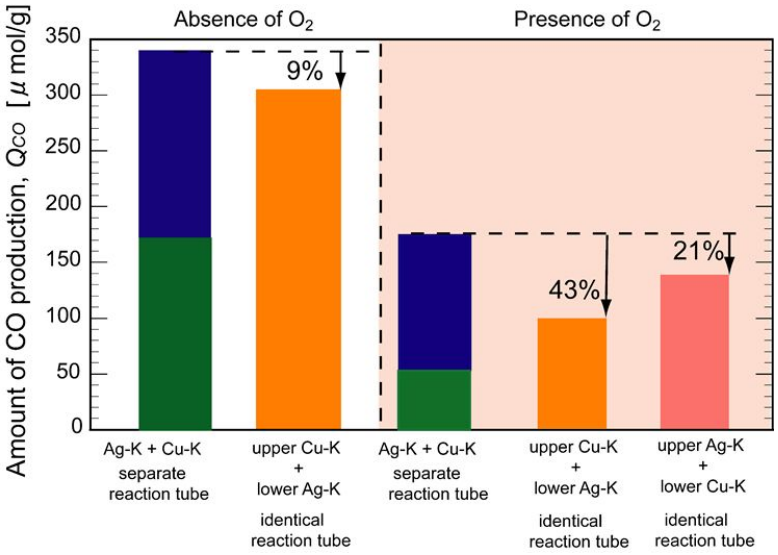

Figure 8. Activity test of Ag-K/Al_2O_3 + Cu-K/Al_2O_3 combined catalyst system

In general, the activity of metallic states is greater than that of oxidized states for hydrogenation reactions using supported metal catalysts; however, the presence of H_2O also negatively influences CCR performance [29]. To develop an understanding of the factors that influence the O_2 compatibility of Ag-K/Al_2O_3, CCR was conducted using a combined Ag- and Cu-K/Al_2O_3 system in the absence or presence of O_2. Cu-K/Al_2O_3 (100 mg) was loaded onto glass wool, which was placed above 100 mg of Ag-K/Al_2O_3, in a tube reactor. The amount of CO formed was compared with the total quantity of CO formed during CCR using 100 mg of Ag- and Cu-K/Al_2O_3 separately (Figure 8). The schematic image of identical reaction tube is shown in Figure S11. In the absence of O_2, the quantity of CO formed during CCR using the combined system was 307 μmol. This value was marginally lower than the total quantity of CO (336 μmol, decreased by 9 %). In contrast, the quantity of CO produced using the combined system was significantly lower (99 μmol) than the total yield of CO in the presence of O_2 (174 μmol, decreased by 43 %). This result was interpreted as the deactivation of Ag-K/Al_2O_3 by in situ generated H_2O from the H_2 reduction of Cu oxides in Cu-K/Al_2O_3. To support this interpretation, the CCR in the presence of O_2 using the opposite order catalyst system (Ag-K/Al_2O_3 catalyst over Cu-K/Al_2O_3) was additionally examined. The quantity of generated CO was 139 mmol/g (Figure 8), which was higher than that for another combined system (99 mmol for Cu-K/Al_2O_3 catalyst over Ag-K/Al_2O_3), supporting the above interpretation. The O_2 compatibility of Ag-K/Al_2O_3 in CCR is mainly ascribed to the suppression of H_2O formation derived from the H_2 reduction of the supported metal species. The supported Ag species are not easily oxidized during the CO_2 adsorption step in the presence of O_2, which suppresses excess H_2O formation in the H_2 reduction step, thereby

preventing the desorption of adsorbed CO_2. Consequently, the adsorbed CO_2 species were effectively reduced to CO using Ag-K/Al_2O_3.

Conclusion

The CCR process was investigated using Ag-K/Al_2O_3 in the absence and presence of O_2 at a relatively low temperature (350 °C). Ag-K/Al_2O_3 enhanced selective CO formation via CCR. CCR performance was maintained even in the presence of O_2 during the CO_2 adsorption step. However, this was not observed in Cu-K/Al_2O_3, which consisted of a homologous element. The results of the XRD and H_2-TPR experiments showed that the supported Ag species in Ag-K/Al_2O_3 was mainly present in the metallic state, even under CO_2+O_2/N_2 flow. In contrast, switching the gas between CO_2+O_2/N_2 and H_2/N_2 resulted in the redox reaction of the supported Cu species in Cu-K/Al_2O_3. This redox property resulted in distinct H_2O formation by alternating CO_2 adsorption in the presence of O_2 and hydrogenation, leading to contrasting CO formation performances during CCR.

Acknowledgement

A part of this study was financially supported by Japan Science and Technology Agency (JST), PRESTO Grant numbers JPMJPR22Q7 and JPMJPR2476, and by KAKENHI (Grant No. JP23H01765) from the Japan Society for the Promotion of Science (JSPS). Z. M. thanks the Iwatani Naoji Foundation.

References

(1) Yuan, Z.; Eden, M. R.; Gani, R. *Ind. Eng. Chem. Res.,* **2016**, *55*, 3383–3419.

(2) Gough, C. *Int. J. Greenhouse Gas Control,* **2008**, *2*, 155–168.

(3) Hong, W. Y. A *CCST* **2022**, *3*, 100044.

(4) Mei, X.; Xu, W. *iScience*, **2023**, *26*, 108499.

(5) Yang, H.; Xu, Z.; Fan, M.; Gupta, R.; Slimane, R. B.; Bland, A. E.; Wright, I. *J. Environ. Sci.,* **2008**, *20*, 14-27.

(6) Peters, M.; Köhler, B.; Kuckshinrichs, W.; Leitner, W.; Markewitz, P.; Müller, T. E. *ChemSusChem*. **2011**, *4*, 1216–1240.

(7) Quadrelli, E. A.; Centi, G.; Duplan, J.-L.; Perathoner, S. *ChemSusChem* **2011**, *4*, 1194–1215.

(8) D'Alessandro, D. M.; Smit, B.; Long, J. R. Carbon Dioxide Capture: Prospects for New Materials. *Angew. Chem. Int. Ed.* **2010**, *49*, 6058–6082.

(9) Bobadilla, L. F.; Riesco-García, J. M.; Penelás-Pérez, G.; Urakawa, A. *J. CO2 Util.* **2016**, *14*, 106–111.

(10) Yu, K. M. K.; Curcic, I.; Gabriel, J.; Tsang, S. C. E. *ChemSusChem*. **2008**, 1, 893–899.

(11) Goeppert, A.; Czaun, M.; Jones, J. P.; Surya Prakash, G. K.; Olah, G. A. *Chem. Soc. Rev*. **2014**, *43*, 7995–8048.

(12) Porosoff, M. D.; Yan, B.; Chen, J. G. *Energy Environ. Sci*. **2016**, *9*, 62–73.

(13) Sun, S.; Sun, H.; Williams, P. T.; Wu, C. *Sustain. Energ. Fuels*, 2021, 5, 4546–4559.

(14) Chen, J.; Xu, Y.; Liao, P.; Wang, H.; Zhou, H. *CCST,* **2022**, *4*. 100052.

(15) Bermejo-López, A.; Pereda-Ayo, B.; González-Marcos, J. A.; González-Velasco, J. R., *Appl. Catal. B* **2019**, *256*. 117845.

(16) Duyar, M. S.; Wang, S.; Arellano-Treviño, M. A.; Farrauto, R. J. *J. CO2 Util.* **2016**, *15*, 65–71.

(17) Li, L.; Wu, Z.; Miyazaki, S.; Toyao, T.; Maeno, Z.; Shimizu, K. *RSC Adv* **2023**, *13*, 2213–2219.

(18) Bobadilla, L. F.; Riesco-García, J. M.; Penelás-Pérez, G.; Urakawa, A. *J. CO2 Util.,* **2016**, *14*, 106–111.

(19) Jo, S. Bin; Woo, J. H.; Lee, J. H.; Kim, T. Y.; Kang, H. I.; Lee, S. C.; Kim, J. C. *Sustain Energy Fuels* **2020**, *4*, 5543–5549.

(20) Shao, B.; Hu, G.; Alkebsi, K. A. M.; Ye, G.; Lin, X.; Du, W.; Hu, J.; Wang, M.; Liu, H.; Qian, F. *Energy Environ. Sci.* **2021**, *14*, 2291–2301.

(21) Li, L.; Zhang, N.; Wu, Z.; Miyazaki, S.; Toyao, T.; Maeno, Z.; Shimizu, K. *Chem. Eng. J.* **2023**, *477*, 147199.

(22) Sasayama, T.; Kosaka, F.; Liu, Y.; Yamaguchi, T.; Chen, S.-Y.; Mochizuki, T.; Urakawa, A.; Kuramoto, K. *J. CO2 Util.* **2022**, *60*, 102049.

(23) Hyakutake, T.; van Beek, W.; Urakawa, A. *J Mater. Chem. A* **2016**, *4*, 6878–6885.

(24) Pinto, D.; van der Bom Estadella, V.; Urakawa, A. *Catal. Sci. Technol.* **2022**, *12*, 5349–5359.

(25) Li, L.; Miyazaki, S.; Yasumura, S.; Ting, K. W.; Toyao, T.; Maeno, Z.; Shimizu, K. *ACS Catal.* **2022**, *12*, 2639–2650.

(26) Baiker, A.; Kilo, M.; Maciejewski, M.; Menzi, S.; Wokaun, A. *Stud. Surf. Sci. Catal.* 1993, 75, 1257–1272.

(27) Liu, H.; Khuan Chuah, G.; Jaenicke, S. *Phys. Chem. Chem. Phys.,* **2015**, *17*, 15012–15018.

(28) Wang, C.; Li, Y.; Zheng, L.; Zhang, C.; Wang, Y.; Shan, W.; Liu, F.; He, H. A, *ACS Catal.* **2021**, *11*, 456–465.

(29) Tatsumichi, T.; Okuno, R.; Hashimoto, H.; Namiki, N.; Maeno, Z. *Green Chem.,* **2024**. 26, 10842-10850.

The data supporting this article are available from the corresponding author upon request